UNIVERSIDAD DE CONCEPCIÓN

Centro de Investigación en Ingeniería Matemática (CI^{2}MA)

Stability analysis and finite volume element discretization for delay-driven spatial patterns in a predator-prey model

Raimund Bürger, Ricardo Ruiz-Baier,
Canrong Tian

PREPRINT 2013-03

SERIE DE PRE-PUBLICACIONES

Stability analysis and finite volume element discretization for delay-driven spatial patterns in a predator-prey model

Raimund Bürger · Ricardo Ruiz-Baier · Canrong Tian

Abstract Time delay is an essential ingredient of spatio-temporal predator-prey models since the reproduction of the predator population after predating the prey will not be instantaneous, but is mediated by some constant time lag for the gestation of predators. Specifically, time delay is considered within a predator-prey reaction-diffusion system. A stability analysis involving Hopf bifurcations with respect to the delay parameter and simulations obtained by a new numerical method reveal how this delay affects the formation of spatial patterns in the distribution of the species. In particular, it turns out that the delay can induce spatial patterns when the carrying capacity of the prey is large. The numerical method consists of a finite volume element (FVE) method for the spatial discretization of the model combined with a Runge-Kutta scheme for its time discretization.

Keywords Spatial patterns · Time delay · Pattern selection · Finite volume element discretization

Mathematics Subject Classification (2000) 35B35 · 35B40 · 65M60 · 92D40

1 Introduction

1.1 Scope

The effect of time delay is fundamental in continuous models of populations of single or multiple species whenever the growth rate of a population does not respond instantaneously to changes in population size. One of the first models with delay was proposed by Volterra (1926), who took into account the delay in response of a population's death rate to changes in population density caused by an accumulation of pollutants in the past. Further causes of response delays include

R. Bürger
CI^{2}MA and Departamento de Ingeniería Matemática, Universidad de Concepción, Casilla 160-C, Concepción, Chile. E-mail: rburger@ing-mat.udec.cl

R. Ruiz-Baier
Modeling and Scientific Computing, MATHICSE, École Polytechnique Fédérale de Lausanne, CH-1015 Lausanne, Switzerland. E-mail: ricardo.ruiz@epfl.ch

C. Tian
Department of Basic Sciences, Yancheng Institute of Technology, Yancheng 224003, China. E-mail: unfoxeses@yahoo.com.cn

differences in resource consumption with respect to age structure, migration and diffusion of populations, gestation and maturation periods, delays in behavioral response to environmental changes, and dependence of a population on a food supply that requires time to recover from grazing (Brauer and Castillo-Chávez, 2001). Within epidemic models, time delays describe the incubation periods of infectious diseases, the infection periods of infective members and the periods of recovered individuals with immunity; see Wang (2009) for an overview. The effect of time delay is broadly discussed in most textbooks on mathematical biology (Renshaw, 1991; Brauer and Castillo-Chávez, 2001; Murray, 2002; Britton, 2003). It is well known that the main consequence of a time delay is oscillatory solution behaviour. For instance, the simple delay differential equation $\mathrm{d}u/\mathrm{d}t = -(\pi/(2\tau))u(t-\tau)$, where τ denotes the delay, has the time-periodic solution $u(t) = A\cos(\pi t/(2\tau))$, where A is a constant (Murray, 2002).

In this work we are interested in criteria for the formation, and numerical methods for the efficient simulation, of spatio-temporal patterns described by a predator-prey model with time delay and diffusion. The model is given by

$$\partial_t u_1 - d_1\Delta u_1 = u_1(a_1 - b_{11}u_1 - b_{12}u_2), \quad (\boldsymbol{x},t) \in \Omega\times\mathcal{T}, \tag{1.1a}$$

$$\partial_t u_2 - d_2\Delta u_2 = u_2\big(-a_2 + b_{21}(u_1)_\tau - b_{22}u_2\big), \quad (\boldsymbol{x},t) \in \Omega\times\mathcal{T}, \tag{1.1b}$$

$$\partial_{\boldsymbol{n}} u_1 = \partial_{\boldsymbol{n}} u_2 = 0, \quad (\boldsymbol{x},t) \in \Sigma_{\mathcal{T}}, \tag{1.1c}$$

$$u_1(\boldsymbol{x},t) = \psi_1(\boldsymbol{x},t), \quad u_2(\boldsymbol{x},t) = \psi_2(\boldsymbol{x},t), \quad (\boldsymbol{x},t) \in \Omega_\tau \tag{1.1d}$$

posed on a finite time interval $\mathcal{T} = (0,T)$ for a fixed $T > 0$, and where $\Sigma_{\mathcal{T}} := (\partial\Omega)\times\mathcal{T}$, $\Omega_\tau := \Omega\times[-\tau,0]$, and $\partial_{\boldsymbol{n}}$ denotes the directional derivative with respect to the outer normal vector $\boldsymbol{n}$ of the boundary $\partial\Omega$ of Ω. Here $u_1 = u_1(\boldsymbol{x},t)$ and $u_2 = u_2(\boldsymbol{x},t)$ are the sought densities of the prey and the predator, respectively. The right-hand side of (1.1b) includes the delay term $(u_1)_\tau := u_1(\boldsymbol{x},t-\tau)$, where the constant $\tau > 0$ is the delay. The homogeneous Neumann boundary condition (1.1c) indicates zero population flux across $\partial\Omega$. Moreover, a_1 is the growth rate of the prey, while a_2 is the death rate of the predator, b_{ii} $(i = 1,2)$ are the rates of intra-specific competition, and b_{12} and b_{21} denote the rates of consumption by predator on prey and mass conversion from prey to predator, respectively. The ratios a_i/b_{ii} $(i = 1,2)$ are environmental carrying capacities, and d_1 and d_2 are diffusion coefficients.

It is one purpose of this paper to study the spatial patterns produced by solutions of (1.1) and the onset of oscillatory solution behaviour through a Hopf bifurcation with respect to the delay τ as a bifurcation parameter. The second purpose is to introduce a new numerical method for the solution of (1.1). Our objective here is to explore how delay determines the stability threshold of the steady state. Moreover, it is pertinent to investigate whether different values of the delay can determine the pattern selections. The present analysis reveals that spatial patterns can be induced by a series of Hopf bifurcation critical points. To the authors' knowledge, this property has not been yet reported in the literature related to spatial patterns.

1.2 Related work

Introductions to delay differential equations are given by Kuang (1993) and Smith (2011); see also Chapter 8 of McKibben (2011). For general introductions to bifurcation theory we mention Chow and Hale (1982) and Hale and Koçak (1991), as well as Hassard et al. (1981) for Hopf bifurcations. In predator-prey systems, delay effects were first considered by Volterra (1931). He showed that under certain conditions, all solutions possess an oscillatory behavior. For the delayed non-spatial predator-prey model, the asymptotic stability of the equilibrium and the periodicity of the solution were investigated (see Cunningham and Wangersky, 1957; May, 1973; Bownds and Cushing, 1975, and the references therein). Analyses of non-spatial variants of (1.1) also include Freedman and Hari Rao (1983); Zhao et al. (1997); Wang and Chen (1997); Ruan and Wei (2003) and Jana et al. (2012). Numerical methods tailored for

these kinds of problems can be found in e.g. Bellen and Zennaro (2003); Hairer and Wanner (2002). We here decide to use stable Runge-Kutta schemes proposed by Koto (2008) (see also Huang, 2009; Huang and Vandewalle, 2012).

For predator-prey models with diffusion, the existence of traveling wave solutions was shown by Murray (1976) and Gopalsamy (1980) for discrete and continuous delays, respectively (although their models differ from (1.1)). For (1.1) and related spatio-temporal models, Gourley et al. (2004) proposed that diffusion and time delays interact in the sense that individuals may be at different points in space at past times. Similarly, Sen et al. (2009) show that the *time* delay may induce *spatial* patterns in the reaction-diffusion system. A version of (1.1) with Beddington-Angelis functional response is studied by Zhang et al. (2011) along with numerical simulations in one space dimension. Tian (2012) studies the formation of delay-induced Turing patterns for a version of (1.1) with a different functional response (the bifurcation theory in that paper is less involved). Bifurcations akin to those studied herein, are also analyzed by Rodrigues et al. (2011) for a fully discrete coupled map lattice predator-prey model. Finite difference methods are employed by Sun et al. (2012) and Wang and Pao (2006).

We study the effects of the time delay by a finite volume element (FVE) approximation of (1.1). This method is a hybrid concept between finite elements and finite volume discretizations that features some desirable properties including the ability to deal with unstructured meshes on arbitrarily shaped domains, the conservativity of inter-element fluxes, and the feasibility of error estimates in L^2 and H^1 norms. The main difficulty is the analysis of the FVE method in the sense that trial and test functions belong to different spaces. FVE methods have historically been applied for flow equations (Cai, 1991; Chou, 1997; Quarteroni and Ruiz-Baier, 2011; Li et al., 2012) and recently for other time-dependent convection-diffusion problems including a sedimentation-consolidation model (Bürger et al., 2012), reactive flows in porous media (Ewing et al., 2000), reaction-diffusion systems (Phongthanapanich and Dechaumphai, 2009) and Brusselator models with cross-diffusion (Lin et al., 2012).

1.3 Outline of the paper

In Section 2 we set up some notation and cite two lemmas from the literature. In Section 3 we show that without delay (i.e., $\tau = 0$), the problem (1.1) does not generate spatial patterns, while in the presence of delay ($\tau > 0$), the formation of spatial patterns is induced. To this end, we first prove (in Section 3.1) by standard arguments that (1.1) admits a unique, positive and uniformly bounded solution for all times. In Section 3.2 we analyze the linear stability of (1.1). We show that when τ exceeds a certain critical value τ^*, then the operator arising from linearization of (1.1) around the non-trivial equilibrium $\boldsymbol{u}^*$ admits successions $\{\tau_n^*\}_{n\in\mathbb{N}_0}$ of purely complex eigenvalues, and that the solutions of the linearized version undergo a Hopf bifurcation at $\boldsymbol{u} = \boldsymbol{u}^*$ whenever $\tau = \tau_n^*$. Next, in Section 3.3, we employ the normal form method and the center manifold theory to analyze the direction of the Hopf bifurcation of solutions of (1.1) (using τ as bifurcation parameter) obtained in Section 3.2. The result is a predictive criterion that discriminates whether the Hopf bifurcations are supercritical or subcritical, respectively, and the corresponding bifurcating periodic solutions on the center manifold are stable (unstable, respectively). In Section 4 we introduce the numerical method for the approximate solution of (1.1), which is based on a FVE spatial discretization (introduced in Section 4.1) combined with a Runge-Kutta method for delay differential equations (see Section 4.2). Numerical results are presented in Section 5. Example 1 (Section 5.2) refers to a simplified version of (1.1), for which an exact solution is available. The recorded error histories indicate that the method converges when discretization parameters are refined. Example 2 (Section 5.3) considers the full model (1.1) on a square. It is illustrated that spatial pattern formation and temporal oscillatory behaviour appear as predicted. Example 3 in Section 5.4 reports similar findings in a disk-shaped domain. Finally, Section 6 collects some conclusions.

2 Preliminaries

Notation 2.1 *Let $0 = \mu_1 < \mu_2 < \cdots \to \infty$ be the eigenvalues of $-\Delta$ on Ω under no-flux boundary conditions, and $\mathcal{E}(\mu_i)$ be the space of eigenfunctions corresponding to μ_i. We define the following space decomposition:*

(i) $\mathcal{X}_{ij} := \{\boldsymbol{c}\cdot\phi_{ij} : \boldsymbol{c} \in \mathbb{R}^2\}$, *where* $\{\phi_{ij}\}$ *is an orthonormal basis of* $\mathcal{E}(\mu_i)$ *for* $j = 1, \ldots, \dim \mathcal{E}(\mu_i)$,
(ii) $\mathcal{X} := \{\boldsymbol{u} = (u_1, u_2)^{\mathrm{T}} \in [C^1(\bar{\Omega})]^2 : \partial_{\boldsymbol{n}} u_1 = \partial_{\boldsymbol{n}} u_2 = 0$ *on* $\partial\Omega\}$. *Thus,*

$$\mathcal{X} = \bigoplus_{i=1}^{\infty} \mathcal{X}_i, \quad \text{where } \mathcal{X}_i = \bigoplus_{j=1}^{\dim \mathcal{E}(\mu_i)} \mathcal{X}_{ij}. \tag{2.1}$$

We will eventually employ the following result (see Theorem 2.1 in Pao, 1992).

Lemma 2.1 *Let $(\tilde{c}_1, \tilde{c}_2)$ and $(\hat{c}_1, \hat{c}_2)$ be a pair of ordered upper and lower solutions of the system (1.1). Then, that system has a unique global solution $(u_1(\boldsymbol{x}, t), u_2(\boldsymbol{x}, t))$ such that $\hat{c}_i \le u_i(\boldsymbol{x}, t) \le \tilde{c}_i$, $i = 1, 2$, for $(\boldsymbol{x}, t) \in \Omega \times [0, \infty)$.*

Furthermore, we will appeal to the following lemma by G.J. Butler (proven in Appendix A of Freedman and Hari Rao, 1983).

Lemma 2.2 (Butler's lemma) *Let $\alpha + \beta < 0$ and $\alpha\beta > \gamma$. Then the real parts of solutions of $\lambda^2 - (\alpha + \beta)\lambda + \alpha\beta - \gamma e^{-\tau\lambda} = 0$ are negative for $\tau < \tau_0$, where $\tau_0 > 0$ is the smallest value for which this equation has a solution with real part zero.*

3 Delay-driven spatial patterns

3.1 Existence of solution

In order to show the global existence of solution of (1.1), it suffices to show that any solution candidate $(u_1(\boldsymbol{x}, t), u_2(\boldsymbol{x}, t))$ must be bounded for all $t > 0$. To this end, we define the quantities

$$\hat{\psi}_i(\tau) := \sup_{(y,s)\in\Omega_\tau} \psi_i(y, s), \quad i = 1, 2.$$

Theorem 3.1 *The initial-boundary value problem (1.1) has a unique solution $(u_1(\boldsymbol{x}, t), u_2(\boldsymbol{x}, t))$ for $T = \infty$. Moreover, the components u_1 and u_2 satisfy the following respective bounds:*

$$0 < u_1(\boldsymbol{x}, t) \le \mathcal{A}_1(\tau) := \max\left\{\frac{a_1}{b_{11}}, \hat{\psi}_1(\tau)\right\}, \tag{3.1}$$

$$0 < u_2(\boldsymbol{x}, t) \le \mathcal{A}_2(\tau) := \max\left\{\frac{1}{b_{22}}\left[b_{21}\max\left\{\frac{a_1}{b_{11}}, \hat{\psi}_1(\tau)\right\} - a_2\right], \hat{\psi}_2(\tau)\right\}. \tag{3.2}$$

Proof It is a standard routine to prove the local existence and uniqueness of solutions of (1.1) for small values of T. We first show the positivity of the local solution $(u_1(\boldsymbol{x}, t), u_2(\boldsymbol{x}, t))$ for some T. We now consider (1.1) for the time interval $\mathcal{T} = (0, \tau)$. Since the initial values are positive, the term $(u_1)_\tau$ is positive and bounded on $\Omega \times (0, \tau)$. By the standard maximum principle for parabolic equations, the local solution $(u_1(\boldsymbol{x}, t), u_2(\boldsymbol{x}, t))$ of (1.1) for $\mathcal{T} = (0, \tau)$ is positive on $\Omega \times (0, \tau]$. Moreover, the bounds (3.1) and (3.2) are valid for $0 < t < \tau$. In a

similar way, we now consider the system formed by (1.1a), (1.1b) and (1.1c) for $\mathcal{T} = (\tau, 2\tau)$ along with the following initial condition:

$$u_1(\boldsymbol{x}, t) = \psi_1(\boldsymbol{x}, t), \quad u_2(\boldsymbol{x}, t) = \psi_2(\boldsymbol{x}, t), \quad (\boldsymbol{x}, t) \in \Omega \times [0, \tau].$$

Then the solution $(u_1(\boldsymbol{x}, t), u_2(\boldsymbol{x}, t))$ of this system is positive on $\Omega \times (\tau, 2\tau]$. By the induction principle, $(u_1(\boldsymbol{x}, t), u_2(\boldsymbol{x}, t))$ is positive and bounded for some T.

Now we show the global existence of the solution $(u_1(\boldsymbol{x}, t), u_2(\boldsymbol{x}, t))$ by the method of upper and lower solutions owing to Lemma 2.1. It is easy to verify that the pairs $(\mathcal{A}_1(\tau), \mathcal{A}_2(\tau))$ and $(0, 0)$ are ordered upper and lower solutions of (1.1). Now the existence theorem of Pao (1992) implies that (1.1) admits a unique global solution $(u_1(\boldsymbol{x}, t), u_2(\boldsymbol{x}, t))$. □

We observe that if the initial values $\psi_i(\boldsymbol{x}, 0)$, $i = 1, 2$, are nonnegative and none of the initial values is identically zero, then the corresponding solution of (1.1) $(u_1(\boldsymbol{x}, t), u_2(\boldsymbol{x}, t))$ is strictly positive on $\Omega \times \mathcal{T}$.

3.2 Linear stability analysis

The system (1.1a), (1.1b) has a nontrivial equilibrium

$$\boldsymbol{u}^* = (u_1^*, u_2^*) = \left(\frac{a_1 b_{22} + a_2 b_{12}}{b_{11} b_{22} + b_{12} b_{21}}, \frac{a_1 b_{21} - a_2 b_{11}}{b_{11} b_{22} + b_{12} b_{21}} \right),$$

which is feasible if we assume that the parameters of the kinetics in (1.1) satisfy

$$a_1 / b_{11} > a_2 / b_{21}. \tag{3.3}$$

We now set $u := u_1 - u_1^*$, $v := u_2 - u_2^*$, substitute $u_1 = u + u_1^*$ and $u_2 = v + u_2^*$ into (1.1), and retain only the linear terms in u and v to obtain

$$\begin{aligned}
&\partial_t u - d_1 \Delta u = -b_{11} u_1^* u - b_{12} u_1^* v, \quad (\boldsymbol{x}, t) \in \Omega_T, \\
&\partial_t v - d_2 \Delta v = b_{21} u_2^* u(t - \tau) - b_{22} u_2^* v, \quad (\boldsymbol{x}, t) \in \Omega_T, \\
&\partial_{\boldsymbol{n}} u = \partial_{\boldsymbol{n}} v = 0, \quad (\boldsymbol{x}, t) \in \Sigma_T, \\
&u(\boldsymbol{x}, t) = \psi_1(\boldsymbol{x}, t) - u_1^*, \quad v(\boldsymbol{x}, t) = \psi_2(\boldsymbol{x}, t) - u_2^*, \quad (\boldsymbol{x}, t) \in \Omega_\tau.
\end{aligned}$$

The linearization of (1.1) around $\boldsymbol{u}^*$ can be therefore expressed by $\partial_t \boldsymbol{u} = (\boldsymbol{D}\Delta + \boldsymbol{J}^*)\boldsymbol{u}$, where $\boldsymbol{D} = \operatorname{diag}(d_1, d_2)$, $\boldsymbol{u} = (u, v)^{\mathrm{T}}$, and

$$\boldsymbol{J}^* = \begin{bmatrix} -b_{11} u_1^* & -b_{12} u_1^* \\ b_{21} u_2^* \mathrm{e}^{-\lambda\tau} & -b_{22} u_2^* \end{bmatrix}$$

(cf., e.g., Smith (2011) for the underlying calculus). Notation 2.1 implies that $\mathcal{X}_i$ is invariant under the operator $\boldsymbol{D}\Delta + \boldsymbol{J}^*$, and λ is an eigenvalue of this operator on $\mathcal{X}_i$ if and only if λ is an eigenvalue of the matrix $-\mu_i \boldsymbol{D} + \boldsymbol{J}^*$. For a fixed index i the characteristic equation of $-\mu_i \boldsymbol{D} + \boldsymbol{J}^*$ is

$$\Delta(\lambda, \tau) := \det(-\mu_i \boldsymbol{D} + \boldsymbol{J}^* - \lambda) = 0. \tag{3.4}$$

In what follows, we fix the index i. A direct calculation shows that

$$\Delta(\lambda, \tau) = \lambda^2 - R_i \lambda + Q \mathrm{e}^{-\lambda\tau}, \tag{3.5}$$

where for sake of brevity, we define

$$R_i := b_{11} u_1^* + b_{22} u_2^* + d_1 \mu_i + d_2 \mu_i > 0, \quad Q := b_{12} b_{21} u_1^* u_2^*. \tag{3.6}$$

Then we have the following result on the existence of delay-driven spatial patterns.

Theorem 3.2 *If* (1.1) *satisfies the assumption* (3.3)*, then the delay can induce spatial patterns.*

(i) If the delay is absent, that is $\tau = 0$*, then the positive equilibrium* $\boldsymbol{u}^*$ *of* (1.1) *is locally asymptotically stable.*
(ii) If the delay is present, that is $\tau \neq 0$*, assume that* $\omega^* < Q^{1/2}$*, where*

$$\omega^* := \frac{1}{\sqrt{2}}\Big(\big[R_i^4 + 4Q^2\big]^{1/2} - R_i^2\Big)^{1/2} \tag{3.7}$$

for R_i *and* Q *as defined in* (3.6)*. Then there exists a critical point*

$$\tau^* = \frac{1}{\omega^*}\arccos\frac{\omega^{*2}}{b_{12}b_{21}u_1^*u_2^*} = \frac{1}{\omega^*}\arccos\frac{\omega^{*2}}{Q}$$

such that the positive equilibrium $\boldsymbol{u}^*$ *is locally asymptotically stable for* $\tau \in [0, \tau^*]$ *and unstable for* $\tau \in (\tau^*, \infty)$*.*

Proof (i) We first show that when $\tau = 0$, there are no spatial patterns. From the above argument, it is sufficient to show all the roots of $\Delta(\lambda, 0)$ have negative real parts. It follows from (3.5) that $\Delta(\lambda, 0) = \lambda^2 - R_i\lambda + Q$. Therefore, by the Descartes rule of sign, the quadratic equation $\Delta(\lambda, 0) = 0$ always has two negative roots.

(ii) By the use of the instability result for delayed differential equations owing to Gopalsamy (1992), in order to prove the instability of the uniform equilibrium, it is sufficient to show that there exist a pure imaginary number $\omega\mathrm{i}$, where $\omega \in \mathbb{R}$ and $\mathrm{i}^2 = -1$, and a real number $\tau > 0$ such that $\Delta(\omega\mathrm{i}, \tau) = 0$. If $\omega\mathrm{i}$ is a root of (3.4), then ω must satisfy the pair of equations

$$-\omega^2 - Q\cos\omega\tau = 0, \quad \omega R_i - Q\sin\omega\tau = 0, \tag{3.8}$$

which leads to the quadratic equation (with respect to ω^2)

$$\omega^4 + R_i^2\omega^2 - Q^2 = 0. \tag{3.9}$$

By the Descartes rule of sign, (3.9) always has a unique positive real root (3.7), and $\Delta(\omega\mathrm{i}, \tau) = 0$ has a pair of simple purely imaginary roots $\pm\omega^*\mathrm{i}$ when

$$\tau_n^* = \frac{1}{\omega^*}\arccos\frac{\omega^{*2}}{Q} + \frac{2n\pi}{\omega^*}, \quad n = 0, 1, \ldots. \tag{3.10}$$

If we set

$$\tau^* := \tau_0^* = \frac{1}{\omega^*}\arccos\frac{\omega^{*2}}{Q},$$

then by Lemma 2.2, $\boldsymbol{u}^*$ is stable for $\tau < \tau^*$. On the other hand, if $\tau \geq \tau^*$, then (3.5) has a unique root on the imaginary axis. By the eigenvalue theory of Ruan and Wei (2003), the sum of orders of the zeros of (3.5) for $\tau > \tau^*$ is equal to that of $\tau = \tau^*$. Then (3.5) for $\tau \in [\tau^*, \infty)$ has roots with positive real parts, which implies that $\boldsymbol{u}^*$ is locally asymptotically unstable for $\tau \geq \tau^*$. □

Theorem 3.3 *Under the assumption* (3.3) *solutions of the problem* (1.1) *undergo a Hopf bifurcation at* $\boldsymbol{u}^*$ *when* $\tau = \tau_n^*$ *for* $n \in \mathbb{N}_0$*.*

Proof We have already shown that $\Delta(\omega \mathrm{i}, \tau) = 0$ has a pair of simple purely imaginary roots $\pm\omega^* \mathrm{i}$ at τ_n^*. Thus, to prove that a Hopf bifurcation occurs at $\tau = \tau_n^*$ for $n = 0, 1, \ldots$, we must still prove the following transversality property:

$$\frac{\mathrm{d}}{\mathrm{d}\tau}\big(\mathrm{Re}(\lambda(\tau))\big)\big|_{\tau=\tau_n^*} > 0, \quad n = 0, 1, \ldots. \tag{3.11}$$

To this end, we substitute $\lambda = \sigma + \omega \mathrm{i}$, $\sigma, \omega \in \mathbb{R}$ into (3.4) to obtain

$$\sigma^2 - \omega^2 - R_i\sigma + \mathrm{e}^{-\sigma\tau} Q \cos\omega\tau = 0, \quad 2\sigma\omega - R_i\omega - \mathrm{e}^{-\sigma\tau} Q \sin\omega\tau = 0.$$

Differentiating these equations with respect to τ yields

$$\begin{aligned}
\big(2\sigma - R_i - \tau \mathrm{e}^{-\sigma\tau} Q\cos\omega\tau\big)\frac{\mathrm{d}\sigma}{\mathrm{d}\tau} - 2\omega\frac{\mathrm{d}\omega}{\mathrm{d}\tau} - \mathrm{e}^{-\sigma\tau} Q(\omega\sin\omega\tau + \sigma\cos\omega\tau) = 0,\\
\big(2\omega + \tau \mathrm{e}^{-\sigma\tau} Q\sin\omega\tau\big)\frac{\mathrm{d}\sigma}{\mathrm{d}\tau} + (2\sigma - R_i)\frac{\mathrm{d}\omega}{\mathrm{d}\tau} + \mathrm{e}^{-\sigma\tau} Q(\sigma\sin\omega\tau - \omega\cos\omega\tau) = 0.
\end{aligned}$$

Substituting $\sigma = 0$ into the above equations, we have

$$\begin{aligned}
(-R_i - \tau Q\cos\omega\tau)\frac{\mathrm{d}\sigma}{\mathrm{d}\tau} - 2\omega\frac{\mathrm{d}\omega}{\mathrm{d}\tau} - Q\omega\sin\omega\tau = 0,\\
(2\omega + \tau Q\sin\omega\tau)\frac{\mathrm{d}\sigma}{\mathrm{d}\tau} - R_i\frac{\mathrm{d}\omega}{\mathrm{d}\tau} - Q\omega\cos\omega\tau = 0.
\end{aligned}$$

Solving the above system of linear equations, we obtain

$$\frac{\mathrm{d}\sigma}{\mathrm{d}\tau} = A^{-1}\begin{vmatrix} Q\omega\sin\omega\tau & -2\omega \\ Q\omega\cos\omega\tau & -R_i \end{vmatrix}, \tag{3.12}$$

where A is the determinant. Substituting $\tau = \tau_n^*$, $\omega = \omega^*$ and (3.8) into (3.12), we obtain $A = R_i^2 + 4\omega^{*2} + \tau^*\omega^{*2}R_i > 0$, and thus

$$\frac{\mathrm{d}\sigma}{\mathrm{d}\tau}\bigg|_{\tau=\tau_n^*,\omega=\omega^*} = \frac{(Q\sin\omega^*\tau_n^*)^2 + 2\omega^{*4}}{A} > 0,$$

which proves (3.11). □

3.3 The direction and stability of the Hopf bifurcation

Let $w_1 := u_1 - u_1^*$, $w_2 := u_2 - u_2^*$ and $\gamma := \tau - \tau_n^*$, so that $\gamma = 0$ is the Hopf bifurcation value of system (1.1). Let us recall the Banach space decomposition (2.1) in Notation 2.1 and re-scale time by $t \to t/\tau$ to normalize the delay. The periodic solution of system (1.1) is equivalent to the solution of the following system

$$\begin{aligned}
\partial_t w_1 &= (\tau_n^* + \gamma)(-d_1\mu_i w_1 - b_{11}u_1^* w_1 - b_{12}u_1^* w_2 - b_{11}w_1^2 - b_{12}w_1 w_2),\\
\partial_t w_2 &= (\tau_n^* + \gamma)\big(-d_2\mu_i w_2 + b_{21}u_2^* w_1(t-1) - b_{22}u_2^* w_2 + b_{21}w_1(t-1)w_2 - b_{22}w_2^2\big).
\end{aligned} \tag{3.13}$$

Next, we use the notation of Hassard et al. (1981) and define $\mathcal{C} = C([0,1], \mathbb{R}^2)$. Then the system (3.13) is transformed into a functional differential equation as

$$\dot{\boldsymbol{w}}(t) = L_\gamma(\boldsymbol{w}_t) + f(\gamma, \boldsymbol{w}_t), \tag{3.14}$$

where $\boldsymbol{w}(t) = (w_1(t), w_2(t))^{\mathrm{T}} \in \mathbb{R}^2$, $\dot{} \equiv \mathrm{d}/\mathrm{d}t$, and $L_\gamma : \mathcal{C} \to \mathbb{R}^2$, $f : \mathbb{R} \times \mathcal{C} \to \mathbb{R}^2$, respectively, are represented by

$$L_\gamma(\boldsymbol{\phi}) = (\tau_n^* + \gamma)\begin{bmatrix} -d_1\mu_i - b_{11}u_1^* & -b_{12}u_1^* \\ 0 & -d_2\mu_i - b_{22}u_2^* \end{bmatrix}\begin{pmatrix} \phi_1(0) \\ \phi_2(0) \end{pmatrix}$$

$$+(\tau_n^*+\gamma)\begin{bmatrix}0 & 0\\ b_{21}u_2^* & 0\end{bmatrix}\begin{pmatrix}\phi_1(-1)\\ \phi_2(-1)\end{pmatrix},$$

$$f(\gamma,\boldsymbol{\phi})=(\tau_n^*+\gamma)\begin{pmatrix}-b_{11}\phi_1^2(0)-b_{12}\phi_1(0)\phi_2(0)\\ b_{21}\phi_1(-1)\phi_2(0)-b_{22}\phi_2^2(0)\end{pmatrix},$$

where $\boldsymbol{\phi}(\theta)=(\phi_1(\theta),\phi_2(\theta))^{\mathrm{T}}\in\mathcal{C}$. By the Riesz representation theorem, there exists a 2×2 matrix, denoted $\eta(\theta,\gamma)$, whose entries are functions of bounded variation such that

$$L_\gamma\boldsymbol{\phi}=\int_{-1}^{0}[\mathrm{d}\eta(\theta,\gamma)]\boldsymbol{\phi}(\theta)\quad\text{for }\boldsymbol{\phi}\in\mathcal{C}.$$

As a matter of fact, we can choose

$$\eta(\theta,\gamma)=(\tau_n^*+\gamma)\begin{bmatrix}-d_1\mu_i-b_{11}u_1^* & -b_{12}u_1^*\\ 0 & -d_2\mu_i-b_{22}u_2^*\end{bmatrix}\delta(\theta)$$
$$+(\tau_n^*+\gamma)\begin{bmatrix}0 & 0\\ b_{21}u_2^* & 0\end{bmatrix}\delta(\theta+1),$$

where δ is a Dirac delta function. For $\boldsymbol{\phi}\in C^1([-1,0],\mathbb{R}^2)$ we define

$$A(\gamma)\boldsymbol{\phi}:=\begin{cases}\dfrac{\mathrm{d}\boldsymbol{\phi}(\theta)}{\mathrm{d}\theta} & \text{if }\theta\in[-1,0),\\ \displaystyle\int_{-1}^{0}[\mathrm{d}\eta(s,\gamma)]\phi(s) & \text{if }\theta=0,\end{cases}$$

$$R(\gamma)\phi:=\begin{cases}0 & \text{if }\theta\in[-1,0),\\ f(\gamma,\phi) & \text{if }\theta=0.\end{cases}$$

Thus, system (3.14) is equivalent to

$$\dot{\boldsymbol{w}}_t=A(\gamma)(\boldsymbol{w}_t)+R(\gamma)(\boldsymbol{w}_t),\tag{3.15}$$

where we define $\boldsymbol{w}_t(\theta):=\boldsymbol{w}(t+\theta)$ for $\theta\in[-1,0]$. Now, for $\boldsymbol{\psi}\in C^1([0,1],(\mathbb{R}^2)^*)$ we define

$$A^*\boldsymbol{\psi}(s):=\begin{cases}-\dfrac{\mathrm{d}\boldsymbol{\psi}(s)}{\mathrm{d}s} & \text{if }s\in[-1,0),\\ \displaystyle\int_{-1}^{0}\psi(-t)\mathrm{d}\eta^{\mathrm{T}}(t,0) & \text{if }s=0,\end{cases}$$

and a bilinear inner product $\langle\cdot,\cdot\rangle$ by

$$\langle\boldsymbol{\psi}(s),\boldsymbol{\phi}(\theta)\rangle=\bar{\boldsymbol{\psi}}(0)\boldsymbol{\phi}(0)-\int_{-1}^{0}\int_{0}^{\theta}\bar{\boldsymbol{\psi}}(\xi-\theta)\,\mathrm{d}\eta(\theta)\boldsymbol{\phi}(\xi)\,\mathrm{d}\xi,\tag{3.16}$$

where $\eta(\theta)=\eta(\theta,0)$. Then $A(0)$ and A^* are adjoint operators. From the discussion in Theorem 3.2, we know that $\pm\omega^*\tau_n^*\mathrm{i}$ are eigenvalues of $A(0)$ and therefore they are also eigenvalues of A^*.

Suppose $\boldsymbol{q}(\theta)=(q_1,q_2)^{\mathrm{T}}\mathrm{e}^{\mathrm{i}\omega^*\tau_n^*}$ is the eigenvector of $A(0)$ corresponding to $\omega^*\tau_n^*\mathrm{i}$. Thus, $A(0)\boldsymbol{q}(\theta)=\omega^*\tau_n^*\mathrm{i}\boldsymbol{q}(\theta)$. Then from the definition of $A(0)$ we have

$$\begin{bmatrix}-d_1\mu_i-b_{11}u_1^*-\mathrm{i}\omega^* & -b_{12}u_1^*\\ b_{21}u_2^*\mathrm{e}^{-\mathrm{i}\omega^*\tau_n^*} & -d_2\mu_i-b_{22}u_2^*-\mathrm{i}\omega^*\end{bmatrix}\begin{pmatrix}q_1\\ q_2\end{pmatrix}=\mathbf{0}.$$

Then we have

$$\boldsymbol{q}(\theta)=\left(1,-\frac{d_1\mu_i+b_{11}u_1^*+\mathrm{i}\omega^*}{b_{12}u_1^*}\right)^{\mathrm{T}}\mathrm{e}^{\mathrm{i}\omega^*\tau_n^*\theta}.$$

Similarly, let $\boldsymbol{q}^*(s) = M(q_1^*, q_2^*)\mathrm{e}^{\mathrm{i}\omega^*\tau_n^* s}$ be the eigenvector of A^* corresponding to $-\mathrm{i}\omega^*\tau_n^*$, where the factor M is determined later. Then by $A^*\boldsymbol{q}^*(s) = -\mathrm{i}\omega^*\tau_n^*\boldsymbol{q}^*(s)$ and the definition of A^*, we have

$$\begin{bmatrix} -d_1\mu_i - b_{11}u_1^* + \mathrm{i}\omega^* & b_{21}u_2^*\mathrm{e}^{\mathrm{i}\omega^*\tau_n^*} \\ -b_{12}u_1^* & -d_2\mu_i - b_{22}u_2^* + \mathrm{i}\omega^* \end{bmatrix} \begin{pmatrix} q_1^* \\ q_2^* \end{pmatrix} = \mathbf{0}.$$

This gives

$$\boldsymbol{q}^*(s) = M\left(\frac{-d_2\mu_i - b_{22}u_2^* + \mathrm{i}\omega^*}{b_{12}u_1^*}, 1\right)\mathrm{e}^{\mathrm{i}\omega^*\tau_n^* s}.$$

To ensure that $\langle \boldsymbol{q}^*(s), \boldsymbol{q}(\theta)\rangle = 1$, we need to determine the value of M. From (3.16), we have

$$\begin{aligned} \frac{1}{\bar{M}} &= (q_1^* q_1 + q_2^* q_2) - \int_{-1}^{0}\int_{\xi=0}^{\theta} \bar{\boldsymbol{q}}^*(\xi-\theta)\,\mathrm{d}\eta(\theta)\boldsymbol{q}(\xi)\,\mathrm{d}\xi \\ &= q_1^*\big(q_1 + \tau_n^*\mathrm{e}^{-\mathrm{i}\omega^*\tau_n^*}(0q_1 + 0q_2)\big) + q_2^*\big(q_2 + \tau^*\mathrm{e}^{-\mathrm{i}\omega^*\tau_n^*}(b_{21}u_2^*q_1 + 0q_2)\big) \\ &= -\frac{d_1\mu_i + d_2\mu_i + b_{11}u_1^* + b_{22}u_2^*}{b_{12}u_1^*} + \tau_n^* b_{21}u_2^*\mathrm{e}^{-\mathrm{i}\omega^*\tau_n^*}. \end{aligned} \tag{3.17}$$

Next we will compute the coordinate to describe the center manifold C_0 at $\gamma = 0$. Let $\boldsymbol{w}_t$ be the solution of (3.15) when $\gamma = 0$, and define

$$z(t) := \langle \boldsymbol{q}^*, \boldsymbol{w}_t\rangle, \quad \boldsymbol{W}(t,\theta) := \boldsymbol{W}\big(z(t), \bar{z}(t), \theta\big) := \boldsymbol{w}_t(\theta) - 2\,\mathrm{Re}\{z(t)\boldsymbol{q}(\theta)\}. \tag{3.18}$$

On the center manifold C_0 we have the Taylor expansion

$$\boldsymbol{W}\big(z(t), \bar{z}(t), \theta\big) = \boldsymbol{W}_{20}(\theta)\frac{z^2}{2} + \boldsymbol{W}_{11}(\theta)z\bar{z} + \boldsymbol{W}_{02}(\theta)\frac{\bar{z}^2}{2} + \boldsymbol{W}_{30}(\theta)\frac{z^3}{6} + \cdots,$$

where z and $\bar{z}$ are local coordinates for the center manifold C_0 in the direction of $\boldsymbol{q}^*$ and $\bar{\boldsymbol{q}}^*$. Note that $\boldsymbol{W}$ is real if $\boldsymbol{w}_t$ is real. We only consider the real solutions. Combining $\gamma = 0$ with (3.18) we have that the solution $\boldsymbol{w}_t \in C_0$ of (3.15) satisfies

$$\begin{aligned} \dot{z}(t) &= \mathrm{i}\omega^*\tau_n^* z + \bar{\boldsymbol{q}}^*(0) f\big(0, W(z,\bar{z},\theta) + 2\,\mathrm{Re}\{z\boldsymbol{q}(\theta)\}\big) \\ &\triangleq \mathrm{i}\omega^*\tau_n^* z + \bar{\boldsymbol{q}}^*(0) f_0(z,\bar{z}), \end{aligned}$$

which we rewrite as $\dot{z}(t) = \mathrm{i}\omega^*\tau_n^* z + g(z,\bar{z})$, where

$$\begin{aligned} g(z,\bar{z}) &= \bar{\boldsymbol{q}}^*(0) f_0(z,\bar{z}) = \bar{\boldsymbol{q}}^*(0) f_0(0, \boldsymbol{w}_t) \\ &= \tau_n^* \bar{M}\,(\bar{q}_1^*, \bar{q}_2^*)\begin{pmatrix} -b_{11}\phi_1^2(0) - b_{12}\phi_1(0)\phi_2(0) \\ b_{21}\phi_1(-1)\phi_2(0) - b_{22}\phi_2^2(0) \end{pmatrix} \end{aligned} \tag{3.19}$$

for $\boldsymbol{\phi} = \boldsymbol{w}_t$. Substituting $\boldsymbol{w}(t) = z\boldsymbol{q}(\theta) + \bar{z}\bar{\boldsymbol{q}}(\theta)$ into (3.19), we have

$$\begin{aligned} g(z,\bar{z}) = \tau_n^*\bar{M}\bar{q}_1^*\big[&-(b_{11}q_1^2 + b_{12}q_1q_2)z^2 - (b_{11}\bar{q}_1^2 + b_{12}\bar{q}_1\bar{q}_2)\bar{z}^2 \\ &- 2(b_{11}|q_1|^2 + b_{12}\,\mathrm{Re}\{q_1\bar{q}_2\})z\bar{z}\big] + \tau_n^*\bar{M}\bar{q}_2^*\big[\big(-b_{22}q_2^2 + b_{21}q_1q_2\mathrm{e}^{-\mathrm{i}\omega^*\tau_n^*}\big)z^2 \\ &+ \big(-b_{22}\bar{q}_2^2 + b_{21}\bar{q}_1\bar{q}_2\mathrm{e}^{\mathrm{i}\omega^*\tau_n^*}\big)\bar{z}^2 + \big(-2b_{22}|q_2|^2 + 2b_{21}\,\mathrm{Re}\{q_1\bar{q}_2\mathrm{e}^{-\mathrm{i}\omega^*\tau_n^*}\}\big)z\bar{z}\big]. \end{aligned} \tag{3.20}$$

Letting

$$g(z,\bar{z}) = g_{20}\frac{z^2}{2} + g_{11}z\bar{z} + g_{02}\frac{\bar{z}^2}{2},$$

and substituting $q_1 = q_2^* = 1$ into (3.20), we have

$$\begin{aligned} g_{20} &= 2\tau_n^*\bar{M}\big[\bar{q}_1^*(-b_{11} - b_{12}q_2) + (-b_{22}q_2^2 + b_{21}q_2\mathrm{e}^{-\mathrm{i}\omega^*\tau_n^*})\big], \\ g_{11} &= 2\tau_n^*\bar{M}\big[\bar{q}_1^*(-b_{11} - b_{12}\,\mathrm{Re}\{q_2\}) + (-b_{22}|q_2|^2 + b_{21}\,\mathrm{Re}\{q_2\mathrm{e}^{\mathrm{i}\omega^*\tau_n^*}\})\big], \end{aligned}$$

$$g_{02} = 2\tau_n^* \bar{M}\left[\bar{q}_1^*(-b_{11} - b_{12}\bar{q}_2) + (-b_{22}\bar{q}_2^2 + b_{21}\bar{q}_2 \mathrm{e}^{\mathrm{i}\omega^*\tau_n^*})\right],$$

where M is defined in (3.17) and

$$q_2 = -\frac{d_1\mu_i + b_{11}u_1^* + \mathrm{i}\omega^*}{b_{12}u_1^*}, \quad q_1^* = \frac{-d_2\mu_i - b_{22}u_2^* + \mathrm{i}\omega^*}{b_{12}u_1^*}.$$

Again, according to Hassard et al. (1981), the Hopf bifurcation periodic solutions of (1.1) at τ_n^* on the center manifold are determined by the following formulas:

$$\begin{aligned}
C_1(0) &= \frac{\mathrm{i}}{2\tau_n^*\omega^*}\left(g_{11}g_{20} - 2|g_{11}|^2 - \frac{|g_{02}|^2}{3}\right),\\
\nu_2 &= -\operatorname{Re}\{C_1(0)\}\left(\operatorname{Re}\left\{\frac{\mathrm{d}\lambda}{\mathrm{d}\tau}(\tau_n^*)\right\}\right)^{-1},\\
\beta_2 &= 2\operatorname{Re}\{C_1(0)\},\\
T_2 &= \frac{1}{\tau_n^*\omega^*}\left(-\operatorname{Im}\{C_1(0)\} + \nu_2 \operatorname{Im}\left\{\frac{\mathrm{d}\lambda}{\mathrm{d}\tau}(\tau_n^*)\right\}\right).
\end{aligned}$$

Here ν_2 determines the direction of the Hopf bifurcation. If $\nu_2 > 0$ ($\nu_2 < 0$, respectively) then the Hopf bifurcations are supercritical (subcritical, respectively) and the bifurcating periodic solutions exist for $\tau > \tau_n^*$ ($\tau < \tau_n^*$, respectively). Again β_2 determines the stability of the bifurcating periodic solutions. The bifurcating periodic solution are stable (unstable) if $\beta_2 < 0$ ($\beta_2 > 0$, respectively). Also, T_2 determines the period of periodic solutions: the period increases (decreases, respectively) if $T_2 > 0$ ($T_2 < 0$, respectively). Thus, we have the following result.

Theorem 3.4 *The Hopf bifurcation of solutions of the system (1.1) at the equilibrium $\boldsymbol{u}^*$ when $\tau = \tau_n^*$ is supercritical (subcritical, respectively) and the bifurcating periodic solutions on the center manifold are stable (unstable, respectively) if* $\operatorname{Re}\{C_1(0)\} < 0$ *(*$\operatorname{Re}\{C_1(0)\} > 0$*, respectively).*

3.4 Global stability of the equilibrium

First we study the global stability of the equilibrium when the delay is absent.

Theorem 3.5 *If (1.1) satisfies (3.3) and we choose $\tau = 0$, then its positive equilibrium $\boldsymbol{u}^*$ is globally asymptotically stable.*

Proof We define $E(t) = E_1(t) + E_2(t)$, where

$$E_i(t) := \int_\Omega b_{3-i,i}\left[u_i - u_i^* - u_i^* \log\left(\frac{u_i}{u_i^*}\right)\right]\mathrm{d}\boldsymbol{x}, \quad i = 1, 2.$$

We now show that $E(t)$ is a Lyapunov functional. It is obvious that $E(t) \geq 0$. We now prove that $\mathrm{d}E(t)/\mathrm{d}t \leq 0$. Differentiating $E_1(t)$ yields

$$\begin{aligned}
\dot{E}_1(t) &= b_{21}\int_\Omega \frac{u_1 - u_1^*}{u_1}\frac{\partial u_1}{\partial t}\,\mathrm{d}\boldsymbol{x}\\
&= b_{21}\int_\Omega \frac{u_1 - u_1^*}{u_1} d_1 \Delta u_1\,\mathrm{d}\boldsymbol{x} + b_{21}\int_\Omega (u_1 - u_1^*)(a_1 - b_{11}u_1 - b_{12}u_2)\,\mathrm{d}\boldsymbol{x}.
\end{aligned}$$

Employing the homogeneous Neumann boundary condition (1.1c), we get

$$\dot{E}_1(t) = -b_{21}d_1u_1^*\int_\Omega \frac{|\nabla u_1|^2}{u_1^2}\mathrm{d}\boldsymbol{x} - b_{21}\int_\Omega (u_1 - u_1^*)\big(b_{11}(u_1 - u_1^*) + b_{12}(u_2 - u_2^*)\big)\,\mathrm{d}\boldsymbol{x}.$$

Analogously, we obtain

$$\dot{E}_2(t) = -b_{12}d_2u_2^*\int_\Omega \frac{|\nabla u_2|^2}{u_2^2}\mathrm{d}\boldsymbol{x} + b_{12}\int_\Omega (u_2-u_2^*)\big(b_{21}(u_1-u_1^*)-b_{22}(u_2-u_2^*)\big)\,\mathrm{d}\boldsymbol{x}.$$

Combining the expressions for $\dot{E}_1(t)$ and $\dot{E}_2(t)$, we have

$$\begin{aligned}\dot{E}(t) = &-b_{21}d_1u_1^*\int_\Omega \frac{|\nabla u_1|^2}{u_1^2}\mathrm{d}\boldsymbol{x} - b_{12}d_2u_2^*\int_\Omega \frac{|\nabla u_2|^2}{u_2^2}\mathrm{d}\boldsymbol{x} - b_{11}b_{21}\int_\Omega (u_1-u_1^*)^2\,\mathrm{d}\boldsymbol{x}\\ &- b_{22}b_{12}\int_\Omega (u_2-u_2^*)^2\,\mathrm{d}\boldsymbol{x} \le 0.\end{aligned}$$

This completes the proof. □

Now we study the global stability of the equilibrium in the presence of delay.

Theorem 3.6 *If the system* (1.1) *satisfies the assumption* (3.3) *and*

$$\max\{b_{12},b_{21}\} \le (b_{11}b_{22})^{1/2}, \tag{3.21}$$

then the positive equilibrium $\boldsymbol{u}^*$ *of* (1.1) *is globally asymptotically stable.*

Proof We now define $F(t) = F_1(t) + F_2(t) + F_3(t)$, where

$$\begin{aligned}F_i(t) &:= \int_\Omega b_{3-i,i}\left[u_i - u_i^* - u_i^*\log\left(\frac{u_i}{u_i^*}\right)\right]\mathrm{d}\boldsymbol{x}, \quad i=1,2,\\ F_3(t) &:= \int_\Omega\int_{t-\tau}^t \frac{b_{11}}{2}\big(u_1(s,\boldsymbol{x})-u_1^*\big)^2\,\mathrm{d}s\,\mathrm{d}\boldsymbol{x}.\end{aligned}$$

It is obvious that $F(t)\ge 0$. In a similar way as for Theorem 3.5, we show that $\dot{F}\le 0$. First, direct computation yields

$$\begin{aligned}\dot{F}_1(t) &= -d_1u_1^*\int_\Omega \frac{|\nabla u_1|^2}{u_1^2}\mathrm{d}\boldsymbol{x} - \int_\Omega (u_1-u_1^*)\big(b_{11}(u_1-u_1^*)+b_{12}(u_2-u_2^*)\big)\,\mathrm{d}\boldsymbol{x},\\ \dot{F}_2(t) &= -d_2u_2^*\int_\Omega \frac{|\nabla u_2|^2}{u_2^2}\mathrm{d}\boldsymbol{x}\\ &\quad + \int_\Omega (u_2-u_2^*)\big(b_{21}(u_1(t-\tau,\boldsymbol{x})-u_1^*)-b_{22}(u_2-u_2^*)\big)\,\mathrm{d}\boldsymbol{x},\\ \dot{F}_3(t) &= \frac{b_{11}}{2}\int_\Omega \big((u_1-u_1^*)^2-(u_1(t-\tau,\boldsymbol{x})-u_1^*)^2\big)\,\mathrm{d}\boldsymbol{x}.\end{aligned}$$

Combining these equations, we obtain

$$\begin{aligned}\dot{F}(t) = &-d_1u_1^*\int_\Omega \frac{|\nabla u_1|^2}{u_1^2}\mathrm{d}\boldsymbol{x} - d_2u_2^*\int_\Omega \frac{|\nabla u_2|^2}{u_2^2}\mathrm{d}\boldsymbol{x}\\ &- \int_\Omega\left[\frac{b_{11}}{2}(u_1-u_1^*)^2 + b_{22}(u_2-u_2^*)^2 + \frac{b_{11}}{2}\big(u_1(t-\tau,\boldsymbol{x})-u_1^*\big)^2\right]\mathrm{d}\boldsymbol{x}\\ &+ \int_\Omega \big[b_{21}\big(u_1(t-\tau,\boldsymbol{x})-u_1^*\big)(u_2-u_2^*) - b_{12}(u_1-u_1^*)(u_2-u_2^*)\big]\,\mathrm{d}\boldsymbol{x}.\end{aligned}$$

Thus, in view of (3.21), it follows that $\dot{F}(t)\le 0$. Therefore, $F(t)$ is a Lyapunov functional and the proof is completed. □

Remark 3.1 Theorem 3.6 implies that if (3.21) holds, then the time delay can not induce spatial patterns.

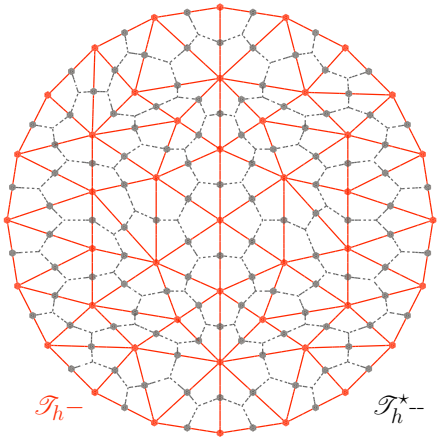

Fig. 1 Primal mesh $\mathscr{T}_h$ and dual mesh $\mathscr{T}_h^*$.

4 Numerical method

4.1 Finite volume element spatial discretization

Let $\mathscr{T}_h$ be a family of partitions of Ω into triangles K, and assume that $\mathscr{T}_h$ with meshsize $h > 0$ is regular in the sense of Ciarlet (1978). By $\mathbb{P}^r(K)$ we denote the space of polynomial functions on $K \in \mathscr{T}_h$ of degree at most $r \geq 0$. The classical finite dimensional space of continuous piecewise linear functions

$$V_h = \big\{v_h \in C^0(\bar{\Omega}) : v_h|_K \in \mathbb{P}^1(K), \forall K \in \mathscr{T}_h\big\},$$

with basis $\{\phi_i\}_i$, is a subspace of $H^1(\Omega)$ used to write the weak formulation in a semi-discrete sense:

$$\begin{aligned}
&\text{For } t > 0, \text{ find } u_{1,h}(t), u_{2,h}(t) \in V_h \text{ such that}\\
&\frac{\mathrm{d}}{\mathrm{d}t}\big(u_{1,h}(t), v_h\big)_\Omega + d_1\big(\nabla u_{1,h}(t), \nabla v_h\big)_\Omega = \big(f_{1,h}(t), v_h\big)_\Omega \quad \forall v_h \in V_h,\\
&\frac{\mathrm{d}}{\mathrm{d}t}\big(u_{2,h}(t), w_h\big)_\Omega + d_2\big(\nabla u_{2,h}(t), \nabla w_h\big)_\Omega
\end{aligned}$$

where the nonlinear reaction terms in the semidiscrete setting are given by

$$\begin{aligned}
f_{1,h}(t) &:= u_{1,h}(t)\big(a_1 - b_{11}u_{1,h}(t) - b_{12}u_{2,h}(t)\big),\\
f_{2,h}(t,\tau) &:= u_{2,h}(t)\big(-a_2 + b_{21}u_{1,h}(\tau) - b_{12}u_{2,h}(t)\big).
\end{aligned}$$

The associated finite volume element discretization is obtained by introducing a dual mesh $\mathscr{T}_h^*$ consisting of polygons (control volumes) K_i^* centered on each node s_i of $\mathscr{T}_h$ and defined by joining the barycenter of each element sharing the vertex s_i and the midpoints of the edges that intersect s_i, see Figure 1.

We next define the finite volume space V_h^* as

$$V_h^* := \big\{w \in L^2(\Omega) : w_{K_i^j} \in \mathbb{P}^0(K_i^*), \forall K_i^* \in \mathscr{T}_h^*\big\},$$

and a Petrov-Galerkin map $\mathcal{P}_h : V_h \to V_h^\star$ (cf., e.g., Quarteroni and Ruiz-Baier, 2011) defined by

$$(\mathcal{P}_h v_h)(x) = \sum_i v_h(s_i)\chi_i(x) \quad \text{for } x \in \Omega,$$

where χ_i is the characteristic function on the control volume $K_i^\star \in \mathscr{T}_h^*$. Using Lemma 3.1 of Lin et al. (2012), we end up with a finite volume element formulation where the only terms recast in the dual space V_h^* appear in the testing of the reactions:

$$\begin{aligned}
&\text{For } t>0, \text{ find } u_{1,h}(t), u_{2,h}(t) \in V_h \text{ such that}\\
&\frac{\mathrm{d}}{\mathrm{d}t}\big(u_{1,h}(t), v_h\big)_\Omega + d_1\big(\nabla u_{1,h}(t), \nabla v_h\big)_\Omega = \big(f_{1,h}(t), \mathcal{P}_h v_h\big)_\Omega \quad \forall v_h \in V_h,\\
&\frac{\mathrm{d}}{\mathrm{d}t}\big(u_{2,h}(t), w_h\big)_\Omega + d_2\big(\nabla u_{2,h}(t), \nabla w_h\big)_\Omega = \big(f_{2,h}(t,\tau), \mathcal{P}_h w_h\big)_\Omega \quad \forall w_h \in V_h.
\end{aligned}$$

Existence and uniqueness of weak solutions to (1.1) along with a-priori estimates can be obtained following Nababan and Teo (1980). The wellposedness of the semidiscrete and fully discrete FVE discretizations and the convergence to the corresponding weak solution will be addressed in a forthcoming contribution. For the moment we will assess the *experimental* convergence properties of the method in Section 5.2.

4.2 Runge-Kutta time discretization

The time interval $\mathcal{T}$ is discretized by nodes $\{t^k\}_{k=-m}^N$, where $t^0 = 0$, $t^{-m} = \tau$ and $t^N = T$. We choose a stable Runge-Kutta time integration scheme (Koto, 2008) yielding the system of equations

$$\begin{aligned}
&\frac{1}{\Delta t}\mathbb{M}\boldsymbol{Y}_i^n + \sum_{j=1}^{i}\alpha_{ij}\mathbb{K}\boldsymbol{Y}_j^n = \frac{1}{\Delta t}\mathbb{M}\boldsymbol{U}^n + \sum_{j=1}^{i-1}\tilde{\alpha}_{ij}\boldsymbol{F}(\boldsymbol{Y}_j^n, \boldsymbol{Y}_j^{n-m}), \quad i=1,\dots,s,\\
&\frac{1}{\Delta t}\mathbb{M}\boldsymbol{U}^{n+1} + \sum_{i=1}^{s}\beta_i\mathbb{K}\boldsymbol{Y}_i^n = \frac{1}{\Delta t}\mathbb{M}\boldsymbol{U}^n + \sum_{i=1}^{s}\tilde{\beta}_i\boldsymbol{F}(\boldsymbol{Y}_i^n, \boldsymbol{Y}_i^{n-m}),
\end{aligned}$$

where s is the order of the Runge-Kutta scheme, $\boldsymbol{U}$ is the vector of nodal values of the discrete solution $(u_{1,h}(t), u_{2,h}(t))$, $\boldsymbol{Y}_i$ is the vector of the discrete solution in the intermediate stage $i \in \{1,\dots,s\}$, $\mathbb{M}$ is the mass matrix with entries $\int_\Omega \phi_i\phi_j\,\mathrm{d}\boldsymbol{x}$, $\mathbb{K}$ is the stiffness matrix with entries $\int_\Omega \nabla\phi_i\cdot\nabla\phi_j\,\mathrm{d}\boldsymbol{x}$, and $\boldsymbol{F}(\boldsymbol{A}^n, \boldsymbol{A}^{n-m})$ is the vector of reaction terms depending on the discrete generic field $\boldsymbol{A}$ at times $t = t^n$ and $t = t^n - \tau = t^{n-m}$. The robustness and performance of Runge-Kutta methods for differential delay equations have been tested e.g. by Bencheva (2010), and theoretical error estimates for advection-diffusion problems are available from Burman and Ern (2012).

5 Numerical results

5.1 Turing parameter space

In view of Theorem 3.2, satisfaction of condition (3.3) is sufficient for the positive uniform equilibrium (u_1^*, u_2^*) to be linearly unstable with respect to the particular case of system (1.1). In order to the numerical simulations, we take the following values in the parameter space

$$a_1 = 2,\ a_2 = 0.2,\ b_{11} = 0.2,\ b_{12} = 0.5,\ b_{21} = 0.2,\ b_{22} = 0.2,\ d_1 = 0.1,\ d_2 = 0.1.$$

For this particular choice, the positive uniform equilibrium is given by

$$(u_1^*, u_2^*) = \left(\frac{25}{7}, \frac{18}{7}\right) \approx (3.5714, 2.5714).$$

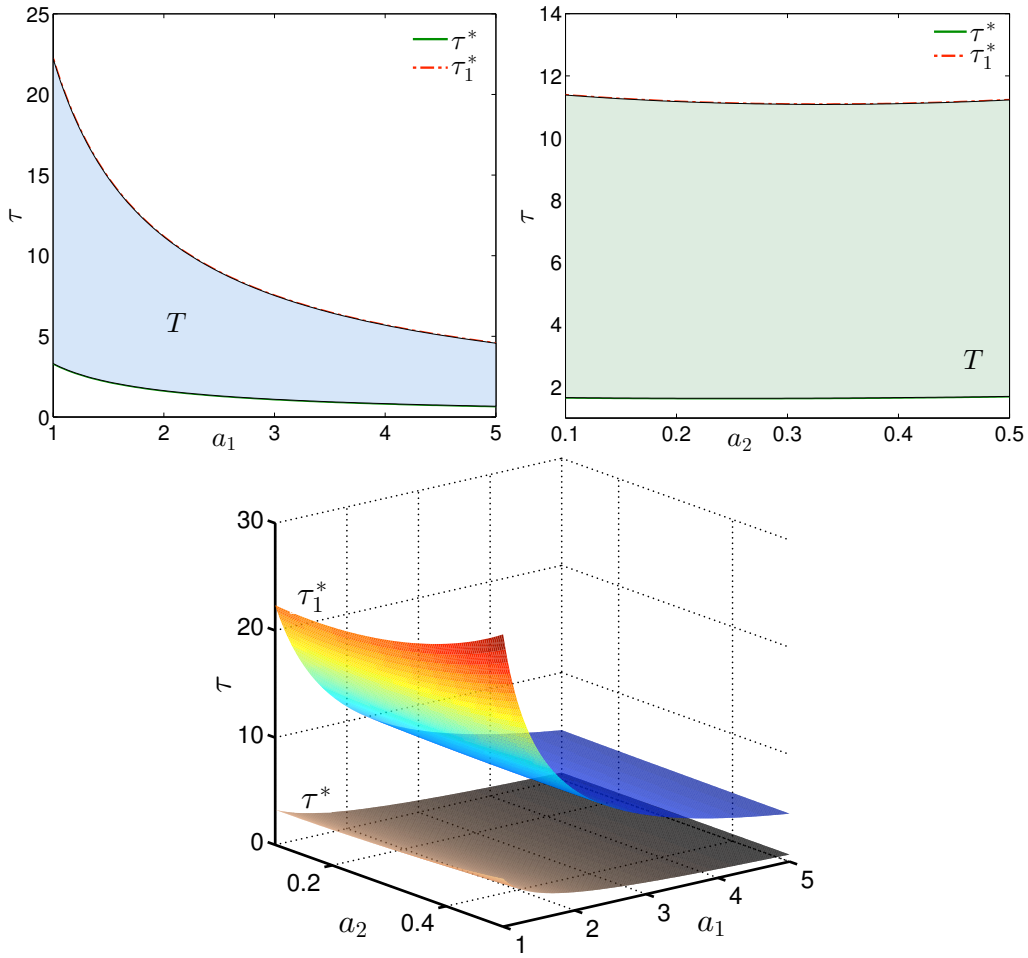

Fig. 2 Bifurcation diagram of model (1.1) for parameters a_1 (top left) and a_2 (top right) where the remaining parameters are set as $b_{11} = 0.2, b_{12} = 0.5, b_{21} = 0.2, b_{22} = 0.2, d_1 = 0.1, d_2 = 0.1$. The figures show the Turing space (labeled as T in the top figures), corresponding to the region bounded by the two Hopf bifurcations $\tau = \tau^* = \tau_0^*$ and $\tau = \tau_1^*$.

These parameters are not the actual values from experimental observations, but they are meaningful from the viewpoint of theoretical biology.

Now, we present the bifurcations represented by the formula (3.10) in the parameter region spanned by the parameters a_1 and τ that are also depicted in Figure 2. All arising spatial patterns are induced in this parameter region.

Following the standard procedure (cf., e.g., Murray, 2003), we can compute the wavenumber explicitly and characterize the pattern selection mechanism by the linearization around the positive uniform equilibrium and taking τ as the Turing bifurcation parameter. From the mathematical viewpoint, the Turing bifurcation occurs when $\mathrm{Im}(\lambda) = 0$ and $\mathrm{Re}(\lambda) > 0$ at $\sqrt{\mu_i}$ for some fixed i. By the eigenvalue theory of the parabolic differential equations, $k_c := \sqrt{\mu_i}$ is the critical wavenumber and λ is the root of the characteristic equation (3.4).

5.2 Example 1: error histories for a simplified model

The accuracy of the numerical method is first studied for the reduced system

$$\partial_t u_1 - \Delta u_1 = -(u_1)_\tau + \frac{u_2}{2}, \quad \partial_t u_2 - \Delta u_2 = -2(u_1)_\tau + u_2,$$

defined on $\Omega = (0, 2\pi)^2$, $t \in [0, 2]$ with homogeneous Neumann boundary conditions and data $u_1(x, y, t) = \cos(x) + \cos(y)$, $u_2(x, y, t) = 2(\cos(x) + \cos(y))$ for $t \in [-\tau, 0]$. Its exact solution is $u_1 = w(t)[\cos(x) + \cos(y)]$, $u_2 = 2u_1$ where

$$w(t) = \begin{cases} 1 & \text{if } -\tau \le t < 0, \\ 1 - t & \text{if } 0 \le t < 1, \\ \frac{1}{2}(t-1)^2 & \text{if } 1 \le t < 2 \end{cases}$$

is a solution of the following delayed ordinary differential equation:

$$\frac{\mathrm{d}w}{\mathrm{d}t} = -w(t-\tau) \quad \text{for } t \in (0, \infty); \quad w(t) = 1 \quad \text{for } t \in [-\tau, 0].$$

A Runge-Kutta scheme of order $s = 2$ will be used, with parameters $\alpha_{21} = 0$, $\alpha_{22} = 1$, $\tilde{\alpha}_{21} = 1$, $\tilde{\alpha}_{22} = 0$, $\beta_1 = 0$, $\beta_2 = 1$, $\tilde{\beta}_1 = 1$, $\tilde{\beta}_2 = 0$ (corresponding to an implicit RK method, see Koto (2008)). When required, the exact solution (if available) is employed as additional initial data. Otherwise, we employ the homogeneous equilibrium state perturbed with a uniformly distributed random field.

For all numerical examples presented herein, we implemented the FVE method on a C++ code based on the FE library Freefem++ (see `www.freefem.org/ff++`) and the visualization has been done with Paraview (`www.paraview.org`).

The observed convergence rates of the approximate solutions are illustrated by computing errors in the $L^2(0, T; H^1(\Omega))$-norm and at the final time $T = 2$ in the $L^2(\Omega)$-norm, defined as

$$e_1(u_i) := \left(\Delta t \sum_{n=-m}^{N} \left\| u_i(t^n) - u_{i,h}^n \right\|_{H^1(\Omega)}^2 \right)^{1/2}, \quad E_0(u_i) := \left\| u_i(t^N) - u_{h,i}^N \right\|_{L^2(\Omega)},$$

for $i = 1, 2$. The spatial accuracy is assessed by performing a series of computations on a set of unstructured primal meshes where each node of a coarser mesh is also present in a finer mesh and the timestep is first fixed to $\Delta t = 10^{-4}$ so that the error in space dominates the error in time. Secondly, we study the time accuracy of the Runge-Kutta scheme by fixing $h = 0.2357$ and running a set of tests with timesteps varying from 10^{-6} to 0.1. We put $\tau = 1$ and the results can be observed in Figure 3 and Table 1, where we report on the errors and experimental orders of convergence of $(\Delta t)^{3/2}$ for $e_1(u_i)$ and of h^2 for $E_0(u_i)$. The sub-optimality of the convergence in time could be explained by the discontinuity of the exact solution $w(t)$.

5.3 Example 2: full delayed predator-prey model on a square

We continue with simulations for system (1.1) modeling a predator-prey scenario where the domain of interest is the square $\Omega = (0, L)^2$ with $L = 60$. The corresponding wavenumber satisfies

$$\boldsymbol{k} = \pi(m_1/L, m_2/L), \quad |\boldsymbol{k}| = \pi\sqrt{(m_1/L)^2 + (m_2/L)^2}, \quad \text{for } m_1, m_2 = 0, 1, \ldots$$

The timestep size is chosen as $\Delta t = 10^{-3}$ and the system is evolved until $T = 1000$. Apart from those given in Section 5.1, different combinations of model parameters have been successfully

h	$E_0(u_1)$	rate	$E_0(u_2)$	rate
3.1221	1.6275	–	3.25517	–
1.6661	4.6691e−1	1.9880	9.3395e−1	1.9845
0.7854	1.1051e−1	1.9163	2.2102e−1	1.9027
0.4158	2.9814e−2	2.0592	5.9629e−2	1.9963
0.2142	9.9176e−3	1.6590	1.9835e−2	1.7102
0.1096	4.8104e−3	1.0803	9.6209e−3	1.2134
Δt	$e_1(u_1)$	rate	$e_1(u_2)$	rate
1e−1	3.4388	–	6.8776	–
1e−2	1.3341e−1	1.4113	2.9113e−1	1.3731
1e−3	5.5459e−2	1.3812	9.4271e−2	1.4912
1e−4	2.0275e−3	1.4370	4.7672e−3	1.2949
1e−5	6.9338e−5	1.4662	1.5713e−4	1.4820
1e−6	2.2986e−6	1.4795	5.6782e−6	1.4421

Table 1 Example 1: Convergence histories for the FVE–Runge-Kutta approximation of the reduced system.

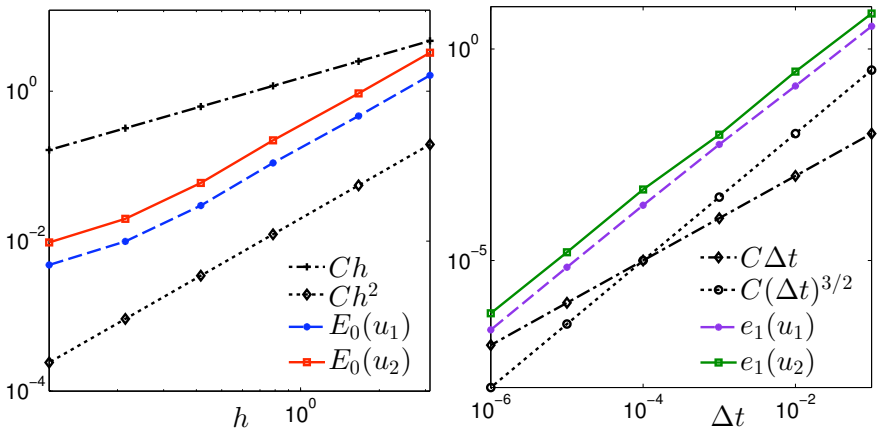

Fig. 3 Example 1: Errors $E_0(u_1), E_0(u_2)$ versus the meshsize (left) and $e_1(\cdot), e_0(\cdot)$ versus the timestep (right) associated to the FVE–Runge-Kutta approximation of the reduced system. See values in Table 1.

tested indicating the significance of the model under various scenarios. From (3.10) we compute the Hopf bifurcation thresholds $\tau^* = 1.6373$ and $\tau_1^* = 11.1749$ and an example for different values of τ is presented in Figures 4 and 5. Periodic solutions should appear due to the Hopf bifurcation. In addition, when the time delay is less than the critical value $\tau^* = 1.6373$, no patterns are generated. For instance, in the top-right plot we see that the initial patterns are smoothed out. From the theoretical results we expect that for $1.8 < \tau < 11.2$ the amplitude of the oscillations will increase significantly within a short period. This is confirmed when we put $\tau = 5$, where we can observe the formation of patterns. This is also the case if we set the time delay as $\tau = \Delta t + \tau^*$. We finally put $\tau = 12$ and notice that spatial patterns appear within a period of around 2τ. This is especially noticed in the bottom-left plot of Figure 5. A similar behavior is observed for a delay $\tau = \Delta t + \tau_1^*$. A primal mesh with 38952 elements and 19733 vertices has been employed. The average number of o GMRES iterations needed to achieve convergence with a tolerance of 10^{-7} was 8.

We compute the fields of maximum and total variations for the species u_j, $j = 1, 2$ at a given point $\boldsymbol{x} \in \Omega$ in $t \in [-\tau, T]$ as

$$\texttt{maxvar}_j(\boldsymbol{x}) := \max_{-m \le k \le N} u_{j,h}^k(\boldsymbol{x}) - \min_{-m \le k \le N} u_{j,h}^k(\boldsymbol{x}),$$

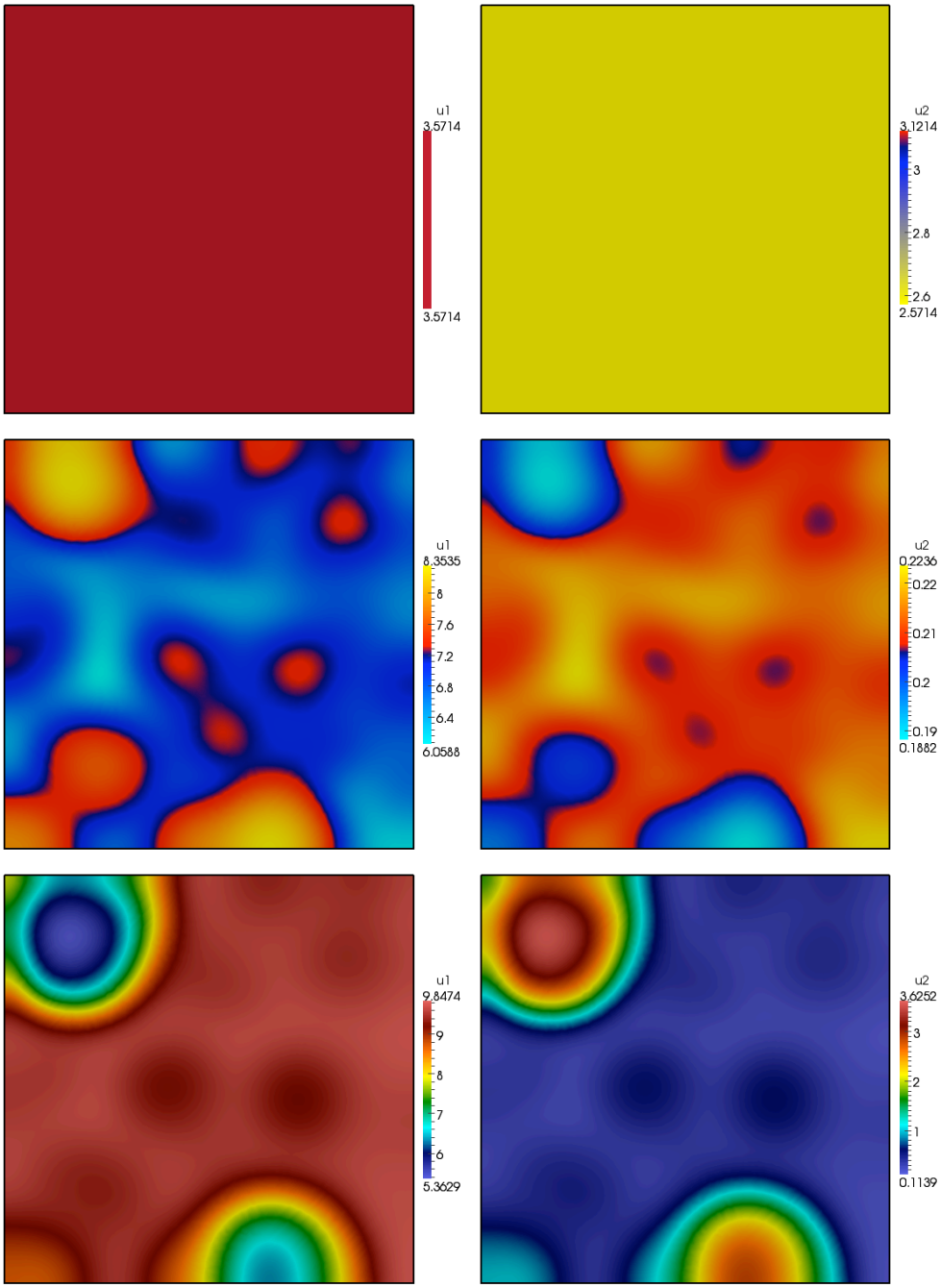

Fig. 4 Example 2: Spatial patterns of species u_1 (left) and u_2 (right) for different time delays $\tau = 1.5, 5, 12$ (respectively, from top to bottom) at $t = 1000$.

$$\texttt{totalvar}_j(\boldsymbol{x}) := \sum_{k=1-m}^{N} \left| u_{j,h}^{k}(\boldsymbol{x}) - u_{j,h}^{k-1}(\boldsymbol{x}) \right|,$$

respectively. These quantities are shown for $\tau = 12$ in Figure 6.

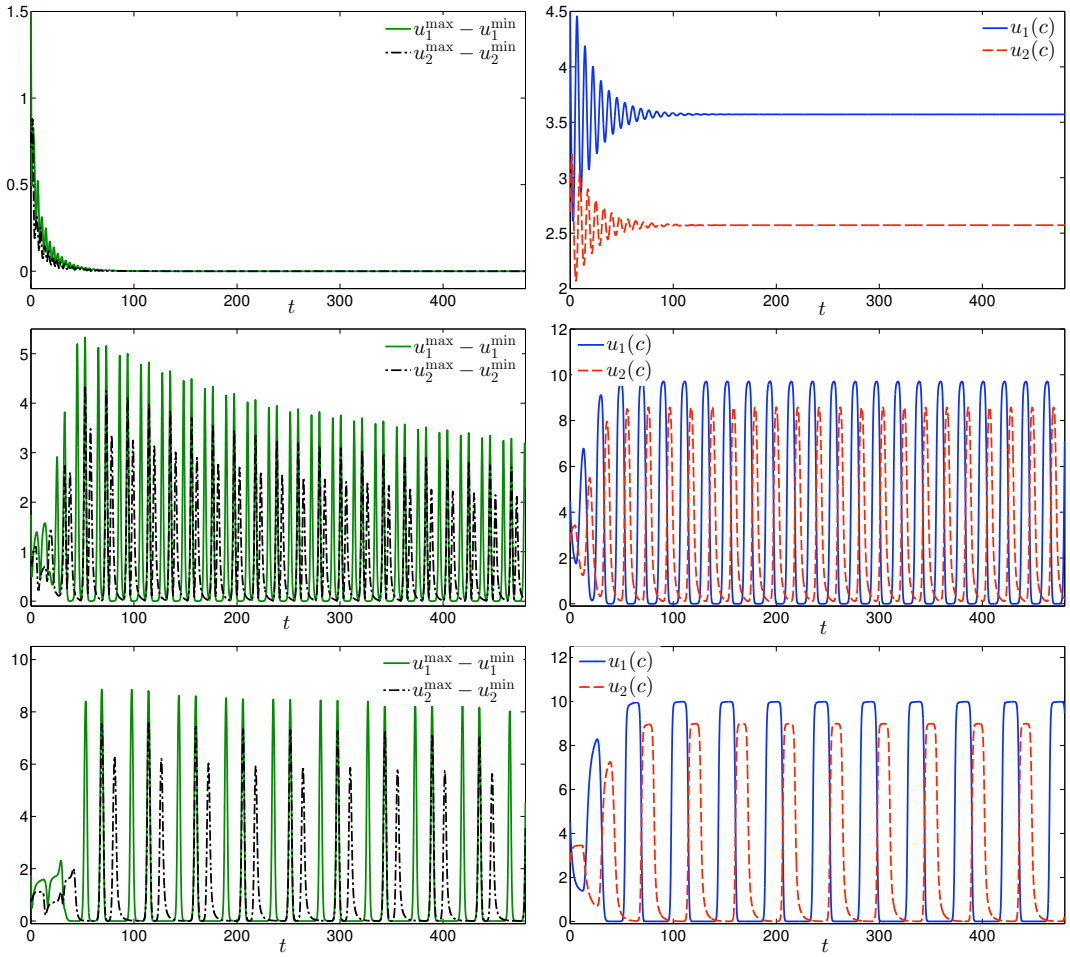

Fig. 5 Example 2: Time evolution of the total variation (left) and density of species on the center c of the domain (right) up to $t = 480$ for different time delays $\tau = 1.5, 5, 12$ (respectively, from top to bottom). When $\tau < \tau^* = 1.6373$, the initial patterns are smoothed out. If $\tau > \tau^*$, patterns appear for the first time, and if $\tau > \tau_1^* = 11.1749$ the patterns appear for the second time. These simulations agree with the sketch in Figure 2.

5.4 Example 3: full delayed predator-prey model on a disk

The patterns can be observed with further detail in a simulation with a smaller wavenumber. The next simulation is then performed on a disk of radius $r = 10$ and Figures 7 and 8 illustrate the behavior of the model for species u_1 and u_2 at time instants $t = 24$ and $t = 480$. These figures show that when the delay τ is close to τ_1^*, the pattern modes are different than those arising when τ is close to τ^*. In this way we are able to numerically reproduce two critical points for the formation of spatial patterns. According to Theorem 3.3, we could obtain, in fact, more than two critical points.

6 Conclusion

In this paper we have presented the theoretical formulation, consistent mathematical analysis, and numerical implementation of pattern formation phenomena in a predator-prey model with delay terms. Applying a stability analysis and suitable numerical simulations, we investigate the Turing parameter space, the Turing bifurcation and the pattern selection. We have shown

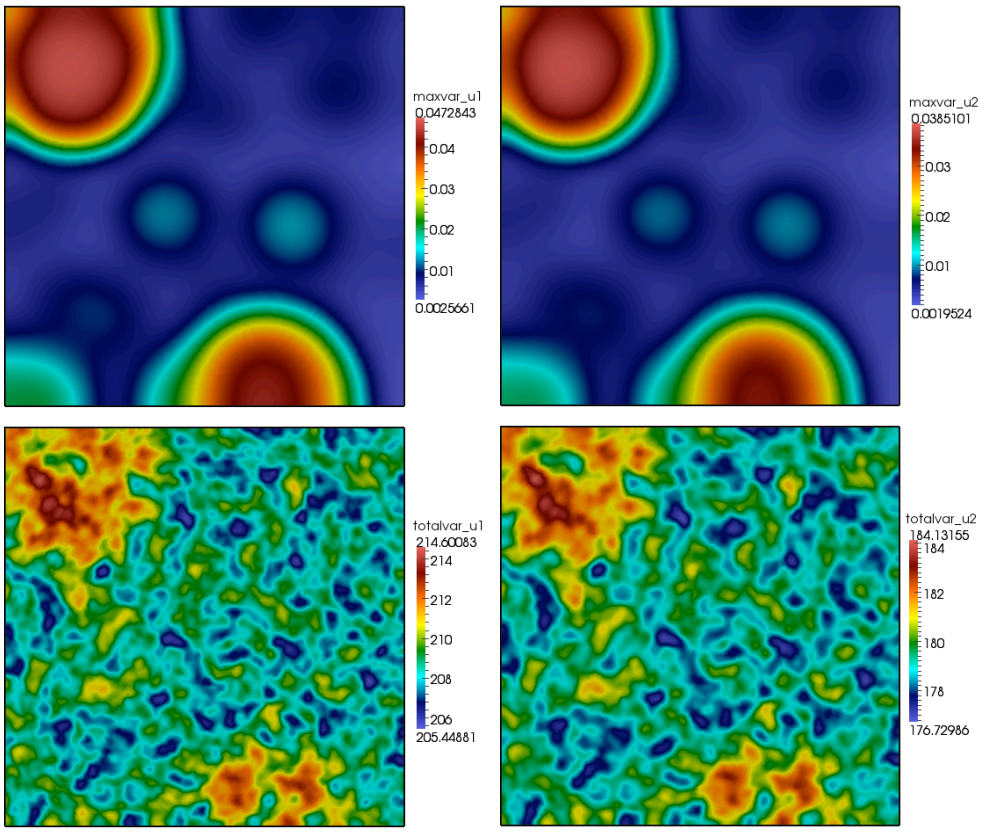

Fig. 6 Example 2: Maximum (top) and total (bottom) variations through time for species u_1 (left) and u_2 (right).

that the time delay can lead to the formation of spatial patterns when the carrying capacity of the prey is large. The stability of the positive uniform equilibrium is determined in the Turing parameter space. From a biological viewpoint, the existence of stability switches induced by the delay is found in the region of the Turing space.

Numerical studies have been employed to support and extend the obtained theoretical results. The numerical simulations illustrate the existence of both stable and unstable equilibrium near the critical point of the delay which is in good agreement with our theoretical analysis results. Our result does not cover yet the case of time delay far away from the critical point. However, numerical simulations show that with increasing the delay from the Hopf bifurcation, the selection of the spatial pattern transform from spots to stripes. At the current stage the present model is still quite simple and can of course accommodate a number of directions for improvement.

Acknowledgements RB acknowledges support by Fondecyt project 1130154; BASAL project CMM, Universidad de Chile and Centro de Investigación en Ingeniería Matemática (CI^2MA), Universidad de Concepción; CONICYT project Anillo ACT1118 (ANANUM); and Red Doctoral REDOC.CTA, project UCO1202 at Universidad de Concepción. RR is supported by the ERC Advanced Grant *Mathcard, Mathematical Modelling and Simulation of the Cardiovascular System*, project 227058. CT acknowledges partial support by the PRC grant NSFC 11201406 and the Qing Lan Project.

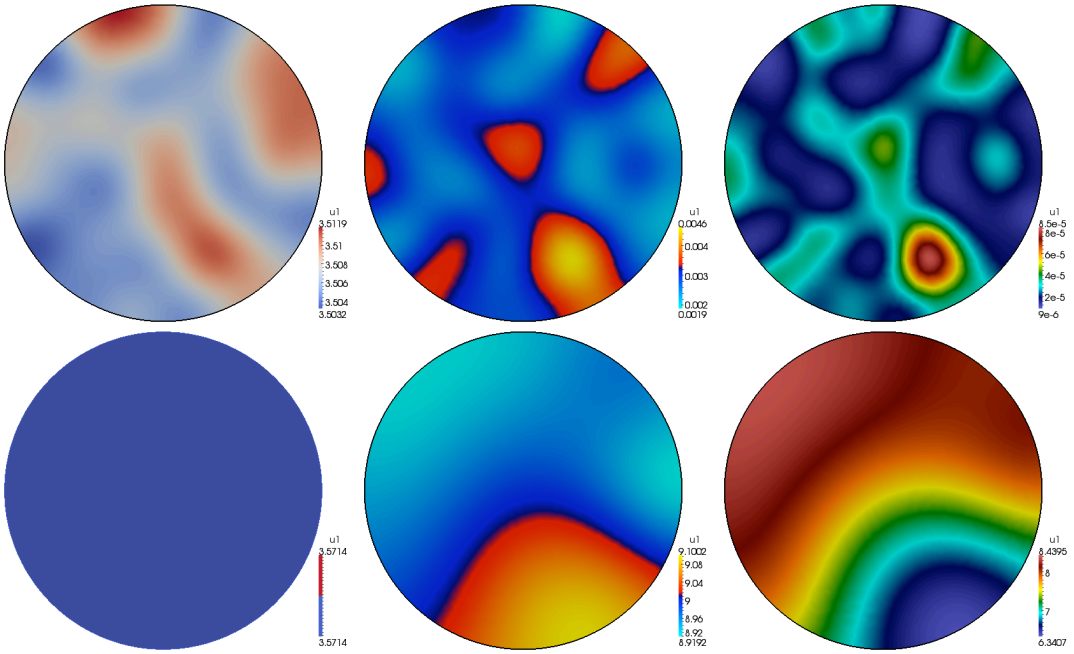

Fig. 7 Example 3: Snapshots of the transient patterns of species u_1 at $t = 24$ (top) and $t = 480$ (bottom) for time delays $\tau = 1.5, 5, 12$ (left, middle and right, respectively).

References

Bellen, A., & Zennaro, M. (2003). *Numerical Methods for Delay Differential Equations*. New York: Clarendon Press, Oxford University Press.

Bencheva, G. (2010). Comparative analysis of solution methods for delay differential equations in hematology. In: Lirkov, I. et al. (eds.): LSSC 2009, Lect. Notes Comput. Sci. vol. 5910, 711–718. New York: Springer.

Bownds, J.M. & Cushing, J.M. (1975). On the behaviour of solutions of predator-prey equations with hereditary terms. *Math. Biosci.*, *26*, 41–54.

Brauer, F., & Castillo-Chávez, C. (2001). *Mathematical Models in Population Biology and Epidemiology*. New York: Springer.

Britton, N.F. (2003). *Essential Mathematical Biology*. London: Springer.

Bürger, R., Ruiz-Baier, R., & Torres, H. (2012). A stabilized finite volume element formulation for sedimentation-consolidation processes. *SIAM J. Sci. Comput.*, *34*, B265–B289.

Burman, E. & Ern, A. (2012). Implicit-explicit Runge-Kutta schemes and finite elements with symmetric stabilization for advection-diffusion equations. *ESAIM: Math. Model. Numer. Anal.*, *46*, 681–707.

Cai, Z. (1991). On the finite volume element method. *Numer. Math.*, *58*, 713-735.

Chou, S.H. (1997). Analysis and convergence of a covolume method for the generalized Stokes problem. *Math. Comput.*, *66*, 85–104.

Chow, S.-N., & Hale, J.K. (1982). *Methods of Bifurcation Theory*. Springer: New York.

Ciarlet, P.G. (1978). *The Finite Element Method for Elliptic Problems*. Amsterdam: North-Holland.

Cunningham, W., & Wangersky, P. (1957). Time lag in prey-predator population models. *Ecology*, *38*, 136–139.

Ewing, R.E., Lazarov, R.D., & Lin, Y. (2000). Finite volume element approximations of non-local reactive flows in porous media. *Numer. Methods Partial Differ. Equ.*, *16*, 285–311.

Freedman, H.I., & Hari Rao, V.S. (1983). The trade-off between mutual interference and time lags in predator-prey system. *Bull. Math. Biol.*, *45*, 991–1004.

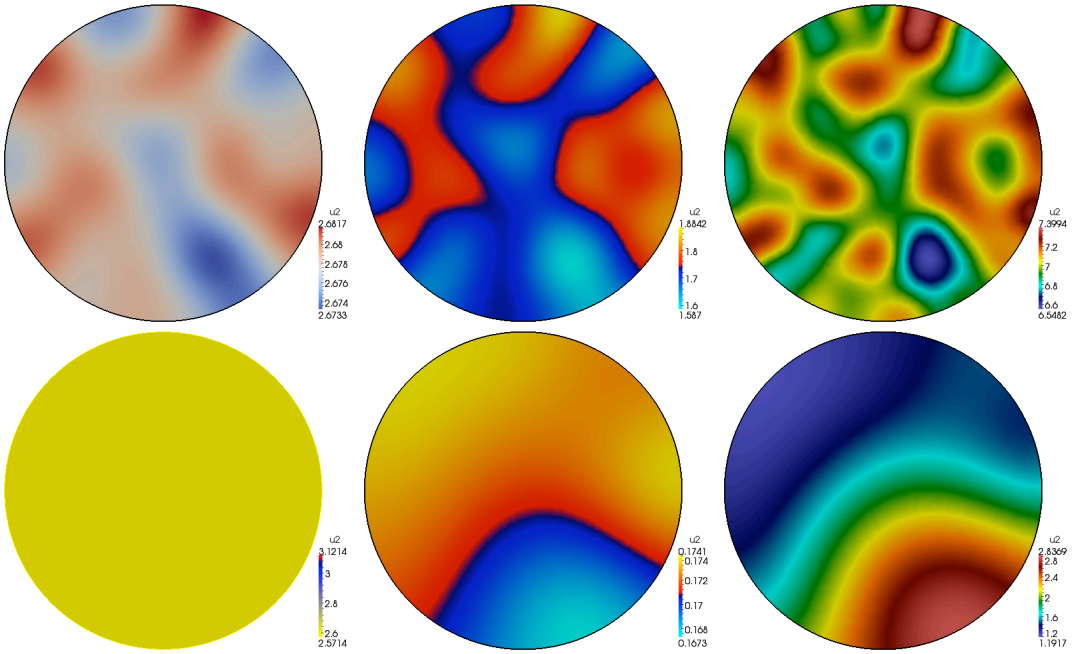

Fig. 8 Example 3: Snapshots of the transient patterns of species u_2 at $t = 24$ (top) and $t = 480$ (bottom) for time delays $\tau = 1.5, 5, 12$ (left, middle and right, respectively).

Gopalsamy, K. (1980). Pursuit evasion wave trains in prey-predator systems with diffusionally coupled delays. *Bull. Math. Biol.*, *42*, 871–887.

Gopalsamy, K. (1992). *Stability and Oscillation in Delay Differential Equations of Population Dynamics*. Dordrecht: Kluwer.

Gourley, S., So, J., & Wu, J. (2004). Nonlocality of reaction-diffusion equations induced by delay: biological modeling and nonlinear dynamics. *J. Math. Sci.*, *124*, 5119–5153.

Hairer, E., & Wanner, G. (2002). *Solving Ordinary Differential Equations II*. New York: Springer.

Hale, J.K., & Koçak, H. (1991). *Dynamics and Bifurcations*. New York: Springer.

Hassard, B., Kazarino, D., & Wan, Y. (1981). *Theory and Applications of Hopf Bifurcation*. Cambridge: Cambridge University Press.

Huang, C. (2009). Delay-dependent stability of high order Runge-Kutta methods. *Numer. Math.*, *111*, 377–387.

Huang, C., & Vandewalle, S. (2012). Unconditionally stable difference methods for delay partial differential equations. *Numer. Math.*, *122*, 579–601.

Jana, S., Chakraborty, M., Chakraborty, K., & Kar, T.K. (2012). Global stability and bifurcation of time delayed prey-predator system incorporating prey refuge. *Math. Comput. Simul.*, *85*, 57–77.

Koto, T. (2008). Stability of IMEX Runge-Kutta methods for delay differential equations. *J. Comput. Appl. Math.*, *211*, 201–212.

Kuang, Y. (1993). *Delay Differential Equations with Applications in Population Dynamics*. New York: Academic Press.

Li, J., Chen, Z., & He, Y. (2012). A stabilized multi-level method for non-singular finite volume solutions of the stationary 3D NavierStokes equations. *Numer. Math.*, *122*, 279–304.

Lin, Z., Ruiz-Baier, R., & Tian, C. (2012). Finite volume element approximation of an inhomogeneous Brusselator model with cross-diffusion. Submitted.

May, R.M. (1973). *Stability and Complexity in Model Ecosystems*. Princeton: Princeton University Press.

McKibben, M.A. (2011). *Discovering Evolution Equations with Applications. Volume 1–Deterministic Equations*. Boca Raton: CRC Press.

Murray, J.D. (1976). Spatial structures in predator-prey communities–A nonlinear time delay diffusional model. *Math. Biosci.*, *30*, 73–85.

Murray, J.D. (2002). *Mathematical Biology I: An Introduction*. Third Edition. New York: Springer.

Murray, J.D. (2003). *Mathematical Biology II: Spatial Models and Biomedical Applications*. Third Edition. New York: Springer.

Nababan, S., & Teo, K.L. (1980). Existence and uniqueness of weak solutions of the Cauchy problem for parabolic delay-differential equations. *Bull. Asutralian Math. Soc.*, *21*, 65–80.

Pao, C.V. (1992). *Nonlinear Parabolic and Elliptic Equations.* New York: Plenum Press.

Phongthanapanich, S., & Dechaumphai, P. (2009). Finite volume element method for analysis of unsteady reaction-diffusion problems. *Acta Mech. Sin.*, *25*, 481–489.

Quarteroni, A., & Ruiz-Baier, R. (2011). Analysis of a finite volume element method for the Stokes problem. *Numer. Math.*, *118*, 737–764.

Renshaw, E. (1991). *Modelling Biological Populations in Space and Time*. Cambridge: Cambridge University Press.

Rodrigues, L.A.D., Mistro, D.C., & Petrovskii, S. (2011). Pattern formation, long-term transients, and the Turing-Hopf bifurcation in a space- and time-discrete predator-prey system. *Bull. Math. Biol.*, *73*, 1812–1840.

Ruan, S.G., & Wei, J.J. (2003). On the zero of some transcendental functions with applications to stability of delay differential equations with two delays. *Dyn. Contin. Discrete Impuls. Sys. Ser. A Math. Anal.*, *10*, 863–874.

Sen, S., Ghosh, P., Riaz, S.S., & Ray, D.S. (2009). Time-delay-induced instabilities in reaction-diffusion systems. *Phys. Rev. E*, *80*, paper 046212.

Smith, H. (2011). *An Introduction to Delay Differential Equations with Applications in the Life Sciences*. New York: Springer.

Sun, G.-Q., Jin, Z., Haque, M., & Li, B.-L. (2012). Spatial patterns of a predator-prey model with cross diffusion. *Nonlinear Dyn.*, *69*, 1631–1638.

Tian, C. (2012). Delay-driven spatial patterns in a plankton allelopathic system. *Chaos*, *22*, paper 013129.

Volterra, V. (1926). Variazioni e fluttuazioni del numero d'individui in specie animali conviventi. *Mem. Acad. Lincei*, *2*, 31–116.

Volterra, V. (1931). *Leçons sur la Théorie Mathématique de la Lutte pour la Vie*. Paris: Gauthier-Villars.

Wang, W. (2009). Epidemic models with time delays. In Z. Ma, Y. Zhou & J. Wu (Eds.), *Modeling and Dynamics of Infectious Diseases* (pp. 289–314). Beijing: Higher Education Press.

Wang, W., & Chen, L.S. (1997). A predator-prey system with stage-structure for predator. *J. Comput. Appl. Math.*, *33*, 83–101.

Wang, Y.-M., & Pao, C.V. (2006). Time-delayed finite difference reaction-diffusion systems with nonquasimonotone functions. *Numer. Math.*, *103*, 485–513.

Zhang, J.-F., Li, W.-T., & Yan, X.-P. (2011). Hopf bifurcation and Turing instability in spatial homogeneous and inhomogeneous predator-prey models. *Appl. Math. Comput.*, *218*, 1883–1893.

Zhao, T., Kuang, Y., & Smith, H.L. (1997). Global existence of periodic solutions in a class of delayed Gause-type predator-prey systems. *Nonlinear Anal.*, *28*, 1373–1390.

Centro de Investigación en Ingeniería Matemática (CI^{2}MA)

PRE-PUBLICACIONES 2012 - 2013

2012-18 Raimund Bürger, Enrique D. Fernández Nieto, El Hadji Koné, Tomás Morales De Luna: *A multilayer shallow water system for polydisperse sedimentation*

2012-19 Fabián Flores-Bazán, Giandomenico Mastroeni: *Strong duality in cone constrained nonconvex optimization: a general approach with applications to nonconvex variational problems*

2012-20 Alfredo Bermúdez, Dolores Gómez, Rodolfo Rodríguez, Pilar Salgado, Pablo Venegas: *Numerical solution of a transient non-linear axisymmetric eddy current model with non-local boundary conditions*

2012-21 Raimund Bürger, Pep Mulet, Luis M. Villada: *Implicit-explicit methods for diffusively corrected multi-species kinematic flow models*

2012-22 Raimund Bürger, Stefan Diehl: *Convexity-preserving flux identification for scalar conservation laws modelling sedimentation*

2012-23 Raimund Bürger, Ilja Kröker, Christian Rohde: *A hybrid stochastic Galerkin method for uncertainty quantification applied to a conservation law modelling a clarifier-thickener unit*

2012-24 Felipe Lepe, David Mora, Rodolfo Rodríguez: *Locking-free finite element method for a bending moment formulation of Timoshenko beams*

2012-25 Raimund Bürger, Pep Mulet, Luis M. Villada: *A diffusively corrected multi-class Lighthill-Whitham-Richards traffic model with anticipation lengths and reaction times*

2012-26 Margareth Alves, Jaime Muñoz-Rivera, Mauricio Sepúlveda, Octavio Vera: *Exponential and the lack of exponential stability in transmission problems with localized Kelvin-Voigt dissipation*

2013-01 Jorge Clarke, Ciprian A. Tudor: *Wiener integrals with respect to the Hermite random field and applications to the wave equation*

2013-02 Julio Aracena, Adrien Richard, Lilian Salinas: *Maximum number of fixed points in AND-OR Boolean network*

2013-03 Raimund Bürger, Ricardo Ruiz-Baier, Canrong Tian: *Stability analysis and finite volume element discretization for delay-driven spatial patterns in a predator-prey model*

Para obtener copias de las Pre-Publicaciones, escribir o llamar a: Director, Centro de Investigación en Ingeniería Matemática, Universidad de Concepción, Casilla 160-C, Concepción, Chile, Tel.: 41-2661324, o bien, visitar la página web del centro: `http://www.ci2ma.udec.cl`







Centro de Investigación en
Ingeniería Matemática (CI²MA)
Universidad de Concepción

Casilla 160-C, Concepción, Chile
Tel.: 56-41-2661324/2661554/2661316
http://www.ci2ma.udec.cl